International Journal of Heat and Mass Transfer 52 (2009) 1085–1093

Contents lists available at ScienceDirect

International Journal of Heat and Mass Transfer

journal homepage: www.elsevier.com/locate/ijhmt

A model for solid bubbles formation in melt–coolant interaction

Leonid A. Dombrovsky

Joint Institute for High Temperatures of the Russian Academy of Sciences, Krasnokazarmennaya 17A, NCHMT, Moscow 111116, Russia

ARTICLE INFO

Article history:
Received 26 June 2008
Received in revised form 25 July 2008
Available online 27 November 2008

Keywords:
Melt droplet
Solidification
Corium
Hollow particles
Bubbles
Fuel–coolant interaction

ABSTRACT

A physical model of formation of thin-wall hollow solid particles in melt–coolant interaction is developed. Such bubble-like solid particles have been observed in the laboratory experiments with some oxide melts and water as a coolant. The considered range of the problem parameters corresponds to interaction of the core melt with water pool in hypothetical severe accident in some industrial nuclear reactors. The calculations showed that only very small corium droplets of diameter less than 1–2 mm can produce "solid bubbles" and it depends on initial overheating of the melt. The results obtained are in qualitative agreement with recently reported laboratory observations.

1. Introduction

The behavior of high-temperature melt droplets in ambient water is an important process in the so-called fuel–coolant interaction (FCI) which takes place in hypothetic severe accident of light-water nuclear reactors. One of the serious engineering problems is an analysis of formation and possible cooling of a particulate debris bed formed by solid corium particles at the bottom of water pool [1–4]. The debris bed composition and the morphology of single particles are very important factors which determine the conditions of debris bed cooling during the heat generation by continuing nuclear reactions.

Recent experimental studies on debris formation with corium simulant materials have shown quite different morphologies of solid particles produced from the melt jet by hydrodynamic and thermal interaction of the jet with water in the pool [5,6]. In previous paper by the author [7], the role of thermal stresses in the crust of solidifying melt particles was analyzed to explain the presence of numerous fragments of thick-wall spherical particles in the debris bed. The present study is focused on another type of particles observed in the experiments by Kudinov et al. [6]: hollow spherical particles of radius $a < 1$ mm with a thin wall of thickness $\delta < 0.1$ mm. Some of these "solid bubbles" were destroyed and the character of the damage looks like a crush under the action high external pressure. As in early paper by Denham et al. [8], the authors of [6] supposed that hollow particles are formed by evaporated water and expanded steam within molten droplets.

The physical picture of possible penetration of small water jets or droplets into the melt drop is not quite clear. One can remember the early paper by Plesset and Chapman [9] containing a model of micro-jet flow generated during asymmetrical collapse of a vapor bubble on the hot surface. A model for interaction of a melt droplet with ambient coolant including penetration of the coolant micro-jets into the droplet of hot molten fuel has been suggested by Buchanan [10]. The photos of solid corium particles with a single orifice [10] were considered by the author as a confirmation of the coolant local penetration into the melt droplets. More recently, Kim and Corradini [11] have proposed a model with an array of micro-jets formed by Taylor instability of the vapor–liquid interface during collapse and regrowth of the vapor film. One can find the details of these models in review by Corradini et al. [12]. The penetration of water micro-jets into the melt particles was also confirmed by morphology of some solidified particles in laboratory experiments by Karbojian et al. [5] and Kudinov et al. [6]. It is especially clear from [6] where numerous small particles of spherical shape with single surface orifices were observed.

In present paper, the penetration of water into the melt particle is not analyzed. We will start our study from the hypothetic presence of small water droplet inside the melt drop. It is natural to assume that characteristic size of water droplet which can appear inside the melt drop is approximately the same as a thickness of collapsed steam film, i.e. the radius of water droplet is in the range between 10 and 50 μm [12,13].

E-mail address: dombr@online.ru

0017-9310/$ - see front matter © 2008 Elsevier Ltd. All rights reserved.
doi:10.1016/j.ijheatmasstransfer.2008.09.024

Nomenclature

a	particle radius
A	coefficient in Eqs. (4) and (5)
B_λ	Planck's function
c	heat capacity
C	coefficient in Eq. (24)
f_v	volume fraction
h	heat transfer coefficient
H	quantity of heat
J	integral defined by Eq. (29)
k	thermal conductivity
L_w	latent heat of evaporation
L_m	latent heat of melting
$\dot{m}$	mass evaporation rate
n	index of refraction
p	pressure
p_λ, P	radiation power
q	heat flux
Q_a	efficiency factor of absorption
r	radial coordinate
r_i	radius of steam cavity
r_w	radius of water droplet
R	coefficient defined by Eq. (21)
R_s	gas constant for steam
t	current time
T	temperature
ΔT	overheating
u	velocity
w_λ, W	normalized radiation power

Greek symbols

α	absorption coefficient
γ	coefficient in Eq. (28)
δ	thickness of solid crust
κ	index of absorption
λ	radiation wavelength
ν, ξ, ζ	coefficients defined by Eq. (7)
ε	hemispherical emissivity
ρ	density
σ	Stefan–Boltzmann constant
σ_θ	circumferential stress
τ	optical thickness
φ	coefficient defined by Eq. (33)
ψ	parameter defined by Eq. (41)

Subscripts and superscripts

cond	conductive
e	external
ex	expansion
f	front of solidification
h	heating
i	interface
m	melt, melting
max	maximum
p	at constant pressure
rad	radiative
s	surface, steam
sol	solidification
t	total
w	water
λ	spectral
0	initial value
$*$	characteristic value

Overbar

–	dimensionless quantity

2. Alternative physical models for interaction of water droplet with ambient high-temperature melt

Let imagine the following initial picture: a spherical water droplet is located in the center of concentric cavity in isothermal high-temperature melt pool. The gap between the droplet and the melt is filled by steam at atmospheric pressure and there is no pressure difference between steam in the cavity and melt in the pool. We will try to describe thermal and hydrodynamic behavior of this system on the basis of various simplified assumptions which lead to some specific model problems. In alternative physical models discussed below, we assume that the melt is optically gray and totally opaque for thermal radiation, whereas steam is perfectly transparent in the near infrared.

In the first physical model (hereafter, model 1), we assume that water droplet does not move in the cavity, i.e. the droplet position in the cavity center is the same from the beginning of the process and up to complete evaporation of the droplet. It is also assumed that the droplet is evaporated from the surface and there are no any perturbations which can destroy the droplet before its complete evaporation. Both thermal radiation from the melt and heat conduction through the steam gap contribute to the droplet evaporation. Of course, one should take into account the steam blowing from the droplet surface. The latter decreases the conductive heat flux at the droplet surface. The evaporation of water and heating of steam is accompanied by expansion of the cavity. The final cavity radius can be easily determined but we should study the dynamics of the cavity expansion.

The second physical model (model 2) is based on the hypothesis of fast internal evaporation and explosion of water droplet due to absorption of a part of high-temperature thermal radiation inside the droplet. Similar effect was observed in misty or cloudy atmosphere while propagating of intense laser radiation [14,15]. The internal absorption of radiation was also discussed as possible cause of fast evaporation of multi-component fuel droplets in diesel engines [16,17]. One should remember some other papers on the effect of internal heating of semi-transparent particles by intense external radiation [18–21]. Most likely, numerous small droplets are produced by "explosion" of the original water droplet, and these secondary droplets are uniformly distributed in the cavity just after the explosion. In is natural to neglect dynamic and thermal nonequilibrium between fine droplets and ambient steam. In other words, the droplets will follow steam during its expansion in the cavity. The further analysis of the problem can be based on the Rayleigh scattering theory for infrared radiative properties of the secondary droplets. It means that absorption of radiation by polydisperse droplets is much greater than scattering and does not depend on droplet size distribution [22]. It is important, that steam containing fine water droplets is not transparent for thermal radiation, but the spectral absorption coefficient of this medium can be easily calculated. Of course, the current volume fraction of water is not uniform due to fast evaporation of water droplets at the periphery of the cavity and the profile of absorption coefficient of the medium has a maximum in the cavity center.

A choice between the above discussed physical models depends on possible internal overheating of the original water droplet irradiated by thermal radiation coming from the ambient melt.

3. Nonuniform heating of water droplet by thermal radiation from the ambient melt

Let us consider the problem of radiative heating of spherical water droplet in concentric cavity in the core melt pool. This model problem is expected to give us an estimate which is important for the choice between two scenarios discussed above. In the case of considerable overheating of water in the droplet center, the model problem #2 might be treated as a realistic one.

We will neglect possible convection in small water droplet and consider only coupled radiation and conduction heat transfer modes. The radiative part of the problem can be formulated on the basis of MDP_0 approximation [23,24]. Moreover, we will use an additional simplification of the problem, which results in the following approximate analytical solution for radial profile of radiation power absorbed in the droplet [25]:

$$P(r)=\frac{3\pi}{r_w}\int_0^\infty w_\lambda(r)\bar{\varepsilon}_\lambda B_\lambda(T_m)d\lambda \quad \bar{\varepsilon}_\lambda=\frac{1}{1/Q_a+(r_w/r_i)^2(1/\varepsilon_m-1)} \tag{1}$$

$$Q_a=\frac{4n_\lambda}{(n_\lambda+1)^2}[1-\exp(-2\alpha_\lambda r_w)] \quad \alpha_\lambda=\frac{4\pi\kappa_\lambda}{\lambda} \tag{2}$$

$$w_\lambda(\bar{r})=\frac{p_\lambda(\bar{r})}{3\int_0^1 p_\lambda(\bar{r})\bar{r}^2d\bar{r}} \quad \bar{r}=r/r_w \tag{3}$$

$$\tau_\lambda\le\tau_\lambda^* \quad p_\lambda=A\frac{\tau_\lambda^*}{\tau_\lambda}\frac{\sinh(2\tau_\lambda)}{\sinh(2\tau_\lambda^*)}(\sinh\tau_\lambda^*+\zeta\cosh\tau_\lambda^*) \tag{4}$$

$$\tau_\lambda>\tau_\lambda^* \quad p_\lambda=A\left[1-\sqrt{1-(\tau_\lambda^*/\tau_\lambda)^2}\right](\sinh\tau_\lambda+\cosh\tau_\lambda) \tag{5}$$

$$A=\frac{4n_\lambda^2\nu}{\nu(\sinh\tau_\lambda^0+\zeta\cosh\tau_\lambda^0)+(\cosh\tau_\lambda^0+\zeta\sinh\tau_\lambda^0)} \tag{6}$$

$$\zeta=\frac{\xi\tanh\tau_\lambda^*-1}{\tanh\tau_\lambda^*-\xi} \quad \xi=\frac{2}{\tanh(2\tau_\lambda^*)}-\frac{1}{\tau_\lambda^*} \quad \nu=\frac{2n_\lambda}{n_\lambda^2+1} \tag{7}$$

$$\tau_\lambda=\alpha_\lambda r \quad \tau_\lambda^0=\alpha_\lambda r_w \quad \tau_\lambda^*=\tau_\lambda^0/n_\lambda \tag{8}$$

For large optical thickness ($\tau_\lambda^0>>1$), Eqs. (4) and (5) can be considerably simplified:

$$\tau_\lambda\le\tau_\lambda^* \qquad p_\lambda=\frac{2n_\lambda^2\nu}{1+\nu}\frac{\tau_\lambda^*}{\tau_\lambda}\exp(2\tau_\lambda-\tau_\lambda^*-\tau_\lambda^0) \tag{9}$$

$$\tau_\lambda>\tau_\lambda^* \qquad p_\lambda=\frac{2n_\lambda^2\nu}{1+\nu}\left[1-\sqrt{1-(\tau_\lambda^*/\tau_\lambda)^2}\right]\exp(\tau_\lambda-\tau_\lambda^0) \tag{10}$$

The radial temperature profiles in water droplet of radius r_w are determined by the following transient radiative–conductive problem:

$$\rho_w c_w\frac{\partial T}{\partial t}=\frac{1}{r^2}\frac{\partial}{\partial r}\left(r^2k_w\frac{\partial T}{\partial r}\right)+P(r) \tag{11}$$

$$T(0,r)=T_s \tag{12}$$

$$\left.\frac{\partial T}{\partial r}\right|_{r=0}=0 \qquad T(t,r_w)=T_s \tag{13}$$

The boundary condition on droplet surface corresponds to equilibrium evaporation of water at saturation temperature T_s. The mass evaporation rate $\dot{m}$ can be found from the energy balance on the droplet surface:

$$\dot{m}=\left(k_w\frac{\partial T}{\partial r}\right)_{r=r_w}/L_{w0} \tag{14}$$

Table 1
Physical parameters used in the calculations.

ρ_w, kg/m^3	1000
c_w, kJ/(kg K)	4
k_w, W/(m K)	0.68
L_{w0}, kJ/kg	2260
$c_{p,s}$, kJ/(kg K)	2.1
k_{s0}, W/(m K)	0.025
R_s, J/(kg K)	462
ρ_m, kg/m^3	8000
c_m, kJ/(kg K)	0.6
k_m, W/(m K)	3
L_m, kJ/kg	400
ε_m	0.85
T_{m0}, K	2850

Eq. (14) does not take into account a contribution of external conductive/convective heat transfer. The effect of surface tension and possible effects of nonequilibrium evaporation are also ignored. The problem statement (11)–(14) should be completed by obvious relation for current radius of the droplet:

$$\dot{r}_w=-\dot{m}/\rho_w \qquad r_w(0)=r_{w0} \tag{15}$$

The dimensionless radial profiles of the radiation power absorbed inside water droplet

$$W(\bar{r})=\frac{P(\bar{r})}{3\int_0^1 P(\bar{r})\bar{r}^2\,d\bar{r}} \tag{16}$$

were calculated at T_m = 3000 K and other physical parameters from Table 1. The numerical results for two limiting cases of the cavity

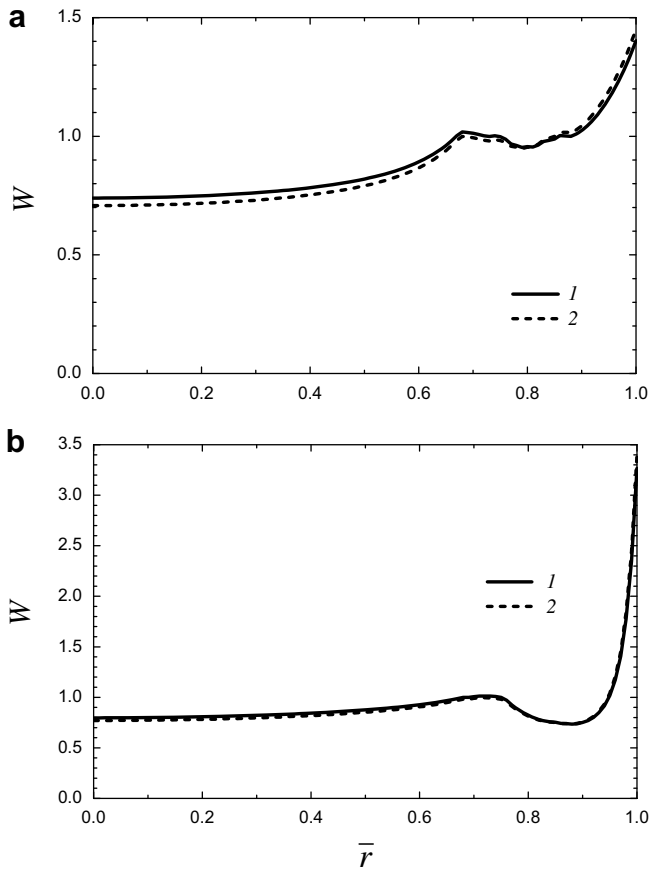

Fig. 1. Normalized radial profiles of the absorbed radiation power inside water droplet: (a) r_w = 10 μm, (b) r_w = 50 μm; *1* – $r_i - r_w << r_w$, *2* – $r_i >> r_w$.

size: $r_i - r_w << r_w$ (thin gap between the droplet and melt) and $r_i >> r_w$ (big cavity) are presented in Fig. 1. The tabulated optical constants of water in the visible and near infrared spectral range from paper by Hale and Querry [26] were used in the calculations. One can see that the difference between two variants of the cavity size is negligible. It is explained by very low value of absorption efficiency factor Q_a in the range of water semi-transparency. As a result, $\bar{\varepsilon}_\lambda \approx Q_a$ and equation (1) can be simplified:

$$P(r) = \frac{3\pi}{r_w}\int_0^\infty w_\lambda(r) Q_a B_\lambda(T_m) d\lambda \tag{17}$$

One can see in Fig. 1 that absolute maximum of absorption takes place near the droplet surface. This effect is explained by significant contribution of infrared radiation in the range of absorption band of water. At the same time, there is a considerable integral absorption of radiation in the internal region of the droplet (far from the surface). The latter is especially important for small droplets. Insignificant contribution of the radiation in the range of water semi-transparency is explained by very small efficiency factor of absorption in this spectral range [27,28]. The calculations showed also that volumetric absorption in the central region of the droplet decreases considerably with the droplet size.

The above formulated transient radiative–conductive problem is complicated due to variation of droplet size by evaporation. One should calculate the radial profile of absorbed radiation power at every time step of the computational procedure. Fortunately, the cavity size makes practically no difference for radiative heating of the droplet.

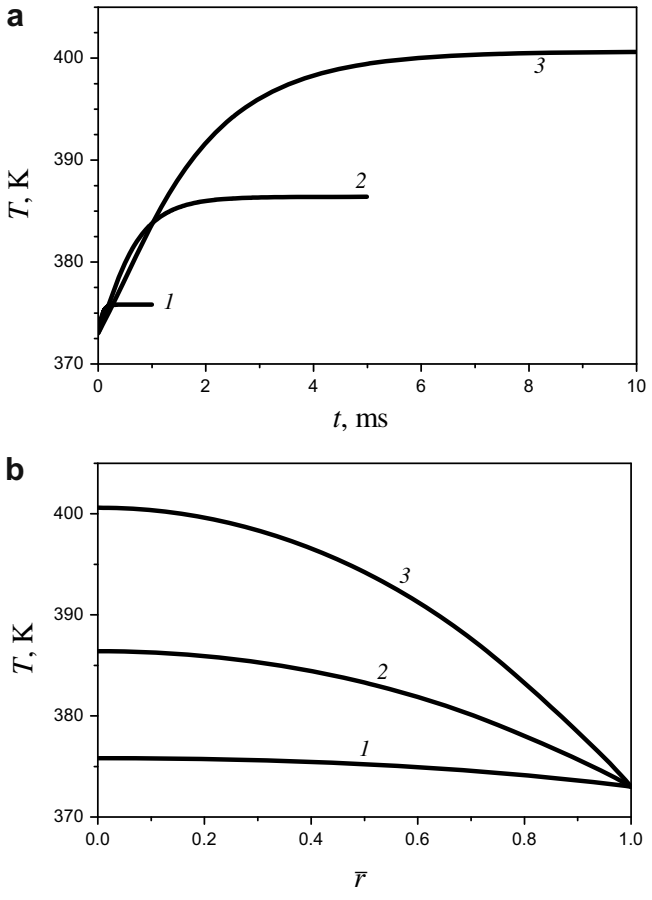

Fig. 2. Temperature in the center of water droplet (a) and steady-state temperature profiles in the droplet (b): *1* – r_w = 10 μm, *2* – 30 μm, *3* – 50 μm.

The upper estimate of water overheating in the central region of the droplet can be obtained from a solution for simplified problem without taking into account the surface evaporation. The numerical results at T_s = 373 K and fixed values of other physical parameters from Table 1 are shown in Fig. 2. One can see that this simple solution does not depend on the details of radial profiles of the absorbed radiation power. The maximal overheating of water $\Delta T \approx 2.8$ K is reached at t_h = 0.2–0.3 ms for small droplet of radius r_w = 10 μm, for larger droplet of radius r_w = 50 μm the corresponding parameters are $\Delta T \approx 28$ K and $t_h \approx 50$ ms.

It is clear that one can employ a simplified transient model based on parabolic approximation for temperature profile as it was done in papers [29,30]. But one should first estimate the surface rate of evaporation. Consider the case of large droplet (r_w = 50 μm). Eqs. (14) and (15) can be written in the form:

$$\dot{r}_w = -\left(k_w \frac{\partial T}{\partial r}\right)_{r=r_w} \Big/ (\rho_w L_{w0}) = -2\frac{k_w}{\rho_w L_{w0}}\frac{\Delta T}{r_w} \tag{18}$$

or

$$\frac{d}{dt}(r_w^2) = -4\frac{k_w \Delta T}{\rho_w L_{w0}} \tag{19}$$

Of course, the value of ΔT is a function of time. But equation (19) enables us to determine the characteristic time of surface evaporation by substituting the average value $\Delta T/2$ instead of initial value of ΔT:

$$t_* = \frac{\rho_w L_{w0} r_{w0}^2}{2k_w \Delta T} \tag{20}$$

Having substituted the values of parameters in Eq. (20) we obtain $t^* \approx 0.15$ s. This value is much greater than the time of droplet heating $t_h \approx 50$ ms.

The above estimate of the evaporation effect is confirmed by complete numerical solution with calculation of the absorbed radiation power at every time step of the computational procedure. The latter is not given here because of the limiting volume of the paper. The complete solution gives the maximal overheating of water $\Delta T_{\max} \approx 27$ K in the center of water droplet of initial radius r_w = 50 μm. This overheating is far from the theoretical maximum $\Delta T^*_{\max} = 320$ K which is given by the homogeneous nucleation theory [31]. Note that conductive heat flux through a thin steam gap increases the surface evaporation rate. It means that the above calculations give an upper estimate for $\Delta T_{\max}$. Therefore, the physical model 2 (droplet explosion in the beginning of the process) seems to be not realistic for pure water.

At the same time, one should remember that very small impurities in water lead to dramatic increase in absorption coefficient in the range of water semi-transparency. The expected results can be estimated by introducing submicron soot particles suspended in water. The spectral absorption coefficient of water containing small particles of soot is calculated as follows:

$$\bar{\alpha}_\lambda = \alpha_\lambda + \frac{\pi f_v}{\lambda} R_\lambda \qquad R_\lambda = \frac{24 n_{soot}\kappa_{soot}}{(n_{soot}^2 - \kappa_{soot}^2 + 2)^2 + 4n_{soot}^2\kappa_{soot}^2} \tag{21}$$

where f_v is the volume fraction of soot, n_{soot} and κ_{soot} are the spectral indices of refraction and absorption of soot, respectively. Eq. (21) can be also rewritten for effective index of absorption:

$$\bar{\kappa}_\lambda = \kappa_\lambda + f_v R_\lambda / 4 \tag{22}$$

According to [27,28], a good estimate for soot in the most important short-wave range can be obtained by assuming the constant value of $R_\lambda = 1$. The resulting approximate equation for effective index of absorption of water containing small soot particles is as follows:

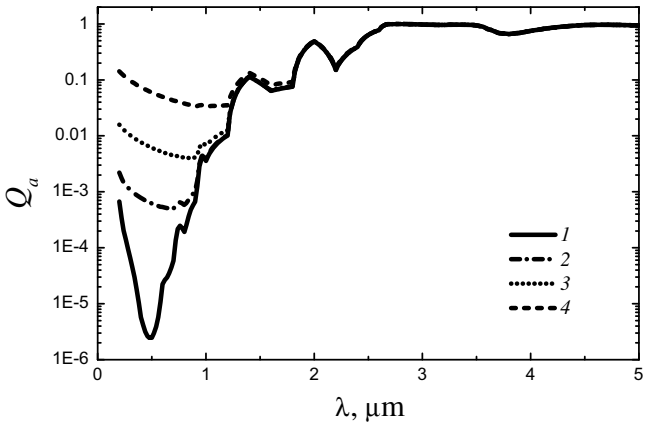

Fig. 3. Spectral variation of absorption efficiency factor for water droplet of radius $r_w = 50$ μm at various volume fractions of soot particles: *1* – $f_v = 0$ (pure water), *2* – $f_v = 10^{-6}$, *3* – $f_v = 10^{-5}$, *4* – $f_v = 10^{-4}$.

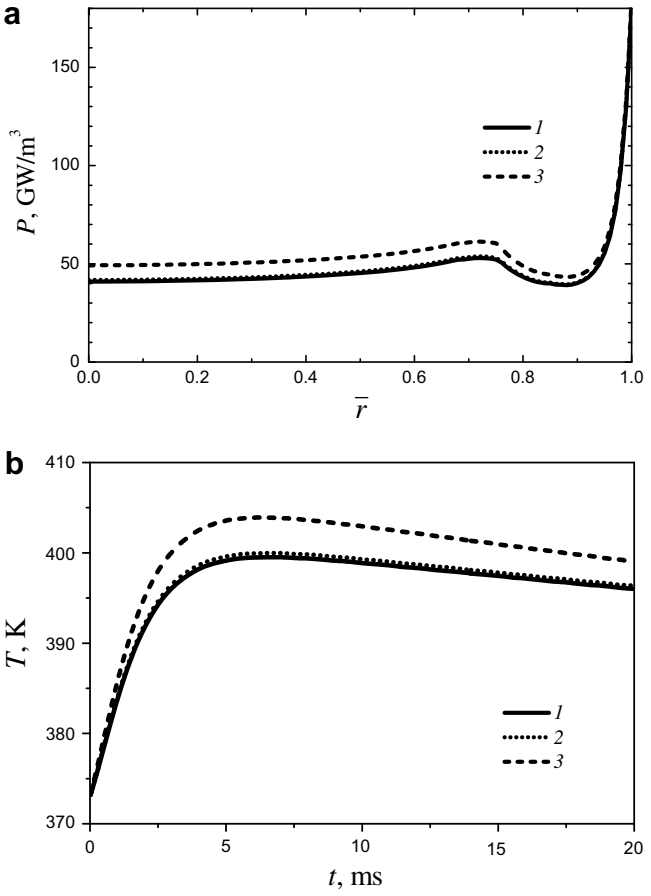

Fig. 4. Effect of soot on profiles of the absorbed radiation power inside water droplet of radius $r_{w0} = 50$ μm (a) and temperature in the center of water droplet (b): *1* – $f_v = 0$ (pure water), *2* – $f_v = 10^{-5}$, *3* – $f_v = 10^{-4}$.

$$\bar{\kappa}_\lambda = \kappa_\lambda + f_v/4 \tag{23}$$

The results of calculations for water containing soot particles are presented in Figs. 3 and 4. One can see that effect of soot on efficiency factor of absorption in the range of water semi-transparency is significant. Nevertheless, only slightly higher absorption of the radiation in water droplet containing soot particles is predicted. As a result, the maximal overheating of water obtained by solving the complete transient problem is weakly sensitive to the presence of large amount of suspended soot. These calculations show that the above conclusion about small internal overheating of water by radiative heating of water droplet is correct not only for pure water but also for "dirty" water. Note that volume fraction of soot $f_v = 10^{-4}$ in water gives $\bar{\alpha}_\lambda \approx 500\ \mathrm{m}^{-1}$ in the visible at wavelength $\lambda = 0.6$ μm. Such suspension is practically opaque in a layer of thickness about 2 cm. It is clear that the role of impurities in radiative heating of water droplet can be ignored. At the same time, possible impurities are very important for nucleation and subsequent intense (explosive) evaporation of water even in the case of small local overheating.

Note that the above calculations give the maximal estimate of internal overheating of water droplet because of significant role of heat conduction through the steam gap to the droplet surface. For this reason, we will not continue the analysis of model 2 but focus on model 1 in subsequent considerations.

4. Equilibrium evaporation of water and isobaric model of steam cavity expansion

The title of this section indicates that the most serious assumption of the model employed is an equilibrium evaporation of the droplet without account for any kinetic effects. It means that variable steam pressure in the cavity is exactly the same as the saturation pressure at current temperature of water droplet. It is known that the equilibrium model is applicable at not to high evaporation rate [32–34]. The latter condition confirmed by calculations is physically clear because of very small efficiency of the radiation absorption by semi-transparent water droplet and effect of steam blowing on heat transfer by conduction through the gap between the droplet and ambient melt.

In the equilibrium calculations, one can use the following analytical approximations for saturation pressure and latent heat of evaporation:

$$\ln\frac{p_s(T)}{p_0} = C\left(\frac{1}{T_0} - \frac{1}{T}\right) \qquad C = 4800\mathrm{K} \tag{24}$$

$$L_w(T) = L_{w0}\left(\frac{T_* - T}{T_* - T_0}\right)^{0.35} \tag{25}$$

where $T_0 = 373$ K, $p_0 = 0.1$ MPa correspond to the initial conditions, and $T^* = 647$ K is the critical temperature of water [31].

The heat balance for isothermal spherical water droplet is as follows:

$$q_t(t) = \frac{\rho_w c_w r_w(t)}{3}\frac{dT_w}{dt} + \dot{m}(t)L_w(T_w) \tag{26}$$

where the total heat flux to the surface of water droplet is

$$q_t = q_{cond} + q_{rad} \quad q_{rad} = \pi\int_0^\infty Q_a B_\lambda(T_m)d\lambda$$

$$q_{cond} = \left(k_s\frac{\partial T}{\partial r}\right)_{r=r_w} \tag{27}$$

The dynamics of steam cavity is determined by the Rayleigh equation:

$$r_i\ddot{r}_i + \frac{3}{2}\dot{r}_i^2 = \frac{p_s - p_0}{\rho_m} \quad r_i(0) = \gamma r_0 \quad \dot{r}_i(0) = 0 \tag{28}$$

where dimensionless parameter $\gamma > 1$ is used instead of initial radius of the cavity.

An additional relation between mass evaporation rate $\dot{m}$, steam pressure p_s, and cavity radius r_i follows from the mass balance:

$$p_s(t)J(t) = p_0 J(0) + R_s\int_0^t \dot{m}r_w^2 dt \quad J(t) = \int_{r_w(t)}^{r_i(t)}\frac{r^2 dr}{T(t,r)} \tag{29}$$

The temperature profile in the steam gap $T(t,r)$ is determined by the following energy equation accompanied by initial and boundary conditions:

$$\rho_s c_{p,s}\frac{\partial T}{\partial t}=\frac{1}{r^2}\frac{\partial}{\partial r}\left(r^2 k_s\frac{\partial T}{\partial r}\right)-\rho_s c_{p,s}u\frac{\partial T}{\partial r} \tag{30}$$

$$T(0,r)=T_w \text{ when } r_0<r<r_{i0} \quad T(0,r)=T_m \text{ when } r=r_{i0} \tag{31}$$

$$T(t,r_w)=T_w \quad T(t,r_i)=T_m \tag{32}$$

at temperature dependent conductivity and density of steam [35,36]:

$$k_s(T)=k_{s0}\left(1+\varphi\frac{T-T_0}{T_0}\right) \quad \varphi=1.83 \quad \rho_s=\frac{p_s}{R_s T} \tag{33}$$

The values of k_{s0} and R_s are given in Table 1. The steam velocity in the last term of Eq. (30) can be estimated as follows:

$$u=\frac{T}{T_m}\frac{r_i^2}{r^2}\dot{r}_i \tag{34}$$

It can be shown that solution for the above formulated problem is characterized by frequent oscillations of all the resulting parameters such as droplet temperature, steam pressure, and cavity radius. As usually, these oscillations are practically symmetric, and time variation of the average parameters (smoothed dependences) can be obtained on the basis of the so-called isobaric model [35], when steam pressure and temperature of water droplet are assumed to be constant: $p_s = p_0$, $T_w = T_0$. In this case, the energy equation for water droplet (26) is radically simplified:

$$\dot{m}(t)=q_t/L_{w0} \tag{35}$$

and we should not use the Rayleigh equation (28) for the cavity dynamics. Instead, it is sufficient to use simple kinematic relation:

$$\dot{r}_i=-\dot{r}_w\frac{\rho_w R_s T_m}{p_0} \tag{36}$$

which follows from the quasi-steady mass balance on the surface of water droplet. A further simplification of the mathematical formulation is reached by neglecting the left-side term in energy equation (30) for steam. It can be shown that this term is really small in comparison with "conductive" and "convective" terms in the right-hand side of Eq. (30). Taking into account Eqs. (34), (36), and (15), the resulting energy equation for steam in the cavity can be written as follows:

$$\dot{m}c_{p,s}r_w^2\frac{\partial T}{\partial r}=\frac{\partial}{\partial r}\left(r^2 k_s\frac{\partial T}{\partial r}\right) \tag{37}$$

It is assumed that condition $\dot{m}\gg\rho_s\dot{r}_w$ in this formulation. Eq. (37) and boundary conditions (32) can be written in dimensionless variables:

$$\psi\frac{\partial\bar{T}}{\partial\bar{r}}=\frac{\partial}{\partial\bar{r}}\left\{\bar{r}^2[1+\varphi(\bar{T}-1)]\frac{\partial\bar{T}}{\partial\bar{r}}\right\} \tag{38}$$

$$\bar{T}(t,1)=1 \quad \bar{T}(t,\bar{r}_i)=\bar{T}_m \tag{39}$$

where

$$\bar{r}=r/r_w \quad \bar{r}_i=r_i/r_w \quad \psi=\frac{\dot{m}c_{p,s}T_0 r_w}{k_{s0}} \quad \bar{T}=T/T_0$$

$$\bar{T}_m=T_m/T_0 \tag{40}$$

Upon integration of (38), this yields:

$$(1-\varphi\bar{q}_{cond})\ln\left[1+\frac{\bar{T}_m-1}{\bar{q}_{cond}}\right]=\psi(1-1/\bar{r}_i)-\varphi(\bar{T}_m-1) \tag{41}$$

where $\bar{q}_{cond}=q_{cond}/q_0$ and $q_0 = k_{s0}T_0/r_w$. Algebraic equation (41) can be used to calculate the value of q_{cond}. The corresponding quasi-steady temperature profile is determined by the following implicit equation:

$$(1-\varphi\bar{q}_{cond})\ln\left[1+\frac{\bar{T}-1}{\bar{q}_{cond}}\right]=\psi(1-1/\bar{r})-\varphi(\bar{T}-1) \tag{42}$$

As a result, we have a complete formulation of the problem based on the isobaric quasi-steady approach suggested above.

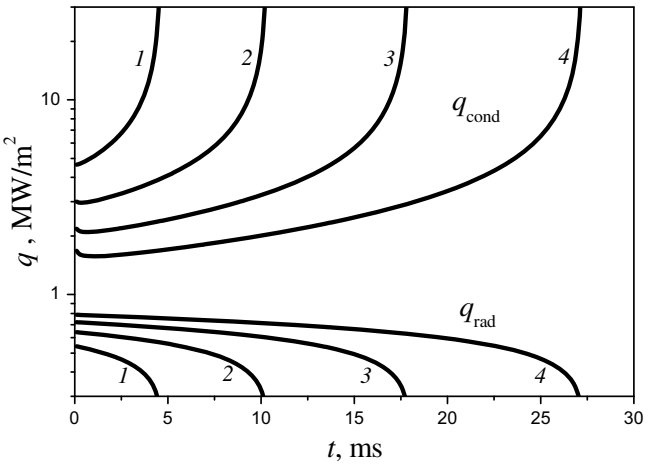

Fig. 5. Time variation of heat flux components at the surface of water droplet: *1* – r_{w0} = 20 μm, *2* – 30 μm, *3* – 40 μm, *4* – 50 μm.

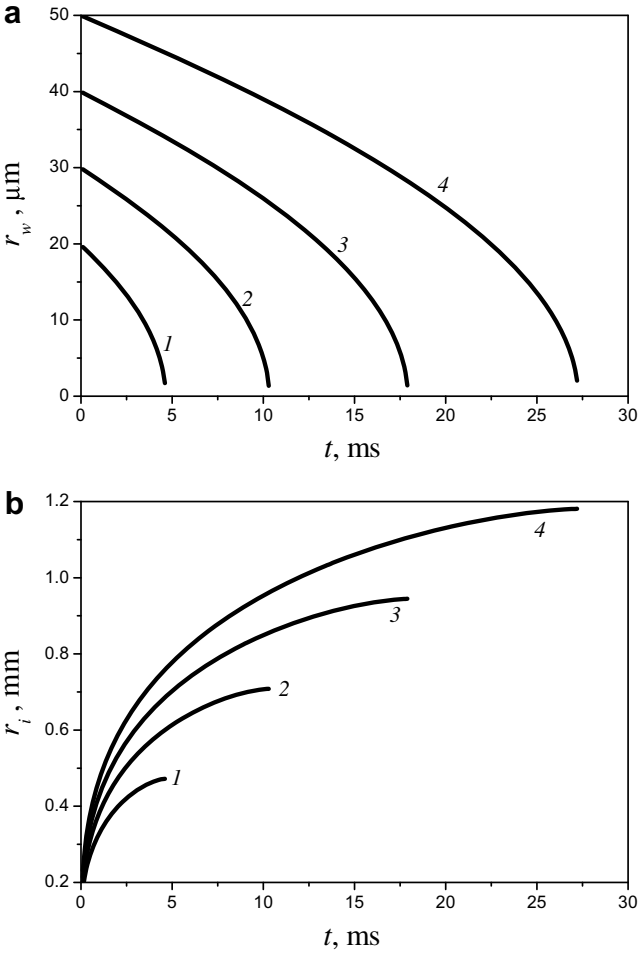

Fig. 6. Time variation of water droplet radius (a) and cavity radius (b): *1* – r_{w0} = 20 μm, *2* – 30 μm, *3* – 40 μm, *4* – 50 μm.

Let us consider some computational results presented in Figs. 5 and 6. The calculations were performed at fixed relative thickness of initial steam blanket $\gamma = r_{i0}/r_{w0} = 1.2$. Additional calculations showed that numerical solution is weakly sensitive to parameter γ. One can see that effect of initial droplet radius is very strong. It is explained by high sensitivity of conductive heat flux to the droplet size. Note that variation of initial radius of water droplet from 20 to 50 μm leads to the calculated range of cavity radius from 0.5 to 1.2 mm. The latter range is a realistic one for hollow particles observed in the experiments [6].

5. Solidification of expanding hollow melt droplet and formation of solid bubble

A variation of the external radius r_e of a hollow melt particle forming from the original melt droplet of radius a can be calculated as follows:

$$r_e(t) = \sqrt[3]{a^3 + r_i^3(t)} \tag{43}$$

Typical dependences $r_e(t)$ at various small values of a are shown in Fig. 7. It goes without saying that Eq. (43) is correct only before melt solidification.

To suggest an adequate model of particle solidification, consider first some physical estimates. The total heat for evaporation of water droplet of radius r_{w0} and heating of steam from temperature T_w to the melt solidification temperature T_{m0} is calculated as follows:

$$H_t = \frac{4}{3}\pi r_{w0}^3 \rho_w [L_{w0} + c_{p,s}(T_{m0} - T_w)] \tag{44}$$

Let us compare the value of H_t and the heat losses by cooling of the melt droplet from temperature $T_{m0}+\Delta T_m$ to T_{m0}:

$$\Delta H_m = \frac{4}{3}\pi a^3 \rho_m c_m \Delta T_m \tag{45}$$

The condition $\Delta H_m = H_t$ leads to the following expression for melt cooling:

$$\Delta T_m = \frac{\rho_w}{\rho_m}\left(\frac{r_{w0}}{a}\right)^3 \frac{L_{w0} + c_{p,s}(T_{m0} - T_w)}{c_m} \tag{46}$$

Eq. (46) gives $\Delta T_m = 1.6$ K at $r_{w0} = 50$ μm even for small corium droplets of radius $a = 0.5$ mm. This result indicates that one can neglect heat losses from the internal surface of hollow melt drop during evaporation of water droplet and heating of steam.

The total heat flux from the external surface of the corium particle is:

$$q_t^e = h(T_{m,s} - T_w) + \varepsilon_m \sigma (T_{m,s}^4 - T_w^4) \tag{47}$$

where $T_{m,s}$ is the surface temperature, h is the convective heat transfer coefficient. Following paper [37], we use the value of $h = 300$ W/(m^2 K) in subsequent calculations (see also recent numerical simulation of film boiling on a sphere by Yuan et al. [38]). Eq. (47) can be approximately written as:

$$q_t^e = h_t(T_{m,s} - T_w) \quad h_t = h + \varepsilon_m \sigma T_{m,s}^3 \tag{48}$$

Let us estimate the melt cooling during expansion of the cavity assuming that initial melt temperature is slightly greater than the melting temperature T_{m0}. We should compare the total heat losses from the particle external surface

$$H_e = 4\pi \int_0^{t_{ex}} q_t^e r_e^2(t) dt \tag{49}$$

where t_{ex} is the expansion time, with the value of ΔH_m determined by Eq. (45). The resulting relation is

$$\Delta T_m = \frac{3h_{t0}(T_{m0} - T_w)}{\rho_m c_m a^3} \int_0^{t_{ex}} r_e^2(t) dt \quad h_{t0} = h + \varepsilon_m \sigma T_{m0}^3 \tag{50}$$

It is convenient to use the following analytical approximation for time dependences of cavity radius presented in Fig. 7:

$$r_i(t) = r_{i0} + (r_{i,\max} - r_{i0})\sqrt[3]{t/t_{ex}} \approx r_{i,\max}\sqrt[3]{t/t_{ex}} \tag{51}$$

This yields:

$$\int_0^{t_{ex}} r_e^2(t) dt = 0.6 a^2 t_{ex} \frac{(1 + \bar{r}_{i,\max}^3)^{5/3} - 1}{\bar{r}_{i,\max}^3}$$

$$\bar{r}_{i,\max} = r_{i,\max}/a \tag{52}$$

Substituting Eq. (52) into Eq. (50) we obtain:

$$\Delta T_m = 1.8(T_{m0} - T_w)\frac{h_{t0} t_{ex}}{\rho_m c_m a} \frac{(1 + \bar{r}_{i,\max}^3)^{5/3} - 1}{\bar{r}_{i,\max}^3} \tag{53}$$

In particular case of $r_{w0} = 50$ μm, Eq. (53) gives $\Delta T_m = 448$ K at $a = 0.5$ mm and $\Delta T_m = 88$ K at $a = 1$ mm. The first value of ΔT_m is much greater than real initial overheating of corium with respect to the melting temperature whereas the second value of ΔT_m is more realistic one. It means that external cooling of small melt

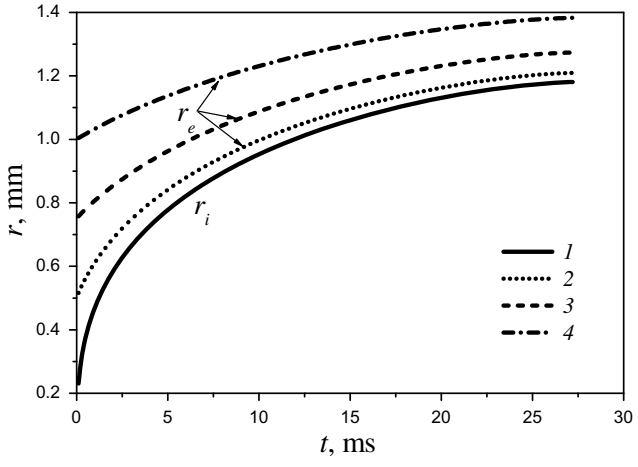

Fig. 7. Time variation of internal (*1*) and external (*2–4*) radii of hollow melt particle during expansion of steam cavity: *2* – $a = 0.5$ mm, *3* – $a = 0.75$ mm, *4* – $a = 1$ mm. Calculations at initial radius of water droplet $r_{w0} = 50$ μm and $\gamma = 1.2$.

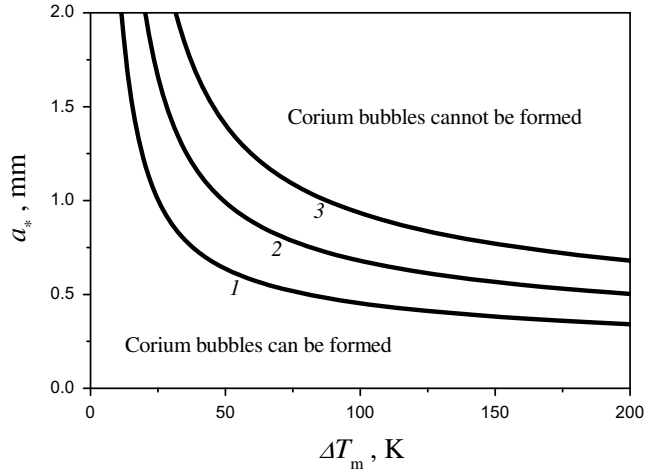

Fig. 8. The conditions of possible formation of hollow solid particles: *1* – $r_{w0} = 30$ μm, *2* – 40 μm, *3* – 50 μm.

droplets of radius $a < a^* \sim 1$ mm will lead to solidification beginning during the cavity expansion. The melt droplets of radius $a > a^*$ will break-up and do not produce hollow solid particles. The dependences $a^*(\Delta T_m)$ presented in Fig. 8 separate the region of possible formation of solid "corium bubbles" from the region where the corium bubbles cannot be formed. One can see that large solid bubbles (formed from melt droplets of radius $a > 2$ μm) can be found only in the case of very small overheating of the melt: $\Delta T_m < 10$–30 K. In the case of $\Delta T_m > 50$ K, only very small corium droplets can produce thin-wall solid particles.

Note that both the velocity of hollow corium particles and the heat flux from these particles to ambient medium are substantially different from the corresponding values for original homogeneous particles. It should be taken into account in CFD calculations of multiphase flow and heat transfer. Particularly, the total thermal radiation power emitted from hollow particles appears to be much greater than that from homogeneous particles of the same mass. The latter effect can be studied on the basis of the Large-Cell Radiation Model (LCRM) [39], which has been recently implemented into the code VAPEX-P for multiphase flow calculations in FCI's [40,41].

In is interesting to compare the conditions of production of solid bubbles from droplets of corium and droplets of simulant melts used in the laboratory experiments. Unfortunately, the physical properties of these melts were not reported in papers [5,6]. Therefore, we use the known properties of alumina melt, which can be found in [37]. Strictly speaking, it is not correct because alumina is semi-transparent in the near infrared and it leads to quite another radiative cooling and solidification of alumina particles [37]. In addition, there is no data in [5,6] for infrared properties of the substances used in the experiments. Nevertheless, we will use the assumption of the melt opacity as it was done for corium to analyze the effect of melting temperature T_{m0} (remember that $T_{m0} = 2320$ K for alumina). The results of calculations are presented in Fig. 9. One can see that the difference between computational results for corium and conventional low-temperature melt is insignificant. It is of the same order of magnitude as the difference between the results for water droplets of radii 40 and 50 μm (see Fig. 8).

Complete solidification of hollow corium particle takes time which is not small due to high value of the latent heat of melting. The particle is expected to be not stable with respect to some external perturbations in the beginning of solidification. Therefore, we should consider the solidification dynamics. The surface rate of melt solidification can be estimated as follows:

$$\frac{d\delta}{dt} = \frac{h_{t0}(T_{m0} - T_w)}{\rho_m L_m} \tag{54}$$

where δ is the thickness of solid crust. The integral emissivity of solid crust is taken to be equal to the melt emissivity. The time of complete solidification is:

$$t_{sol} = \frac{\rho_m L_m \left(\sqrt[3]{a^3 + r_{i,\max}^3} - r_{i,\max} \right)}{h_{t0}(T_{m0} - T_w)} \tag{55}$$

We assume here that appearance of thin crust layer cannot stop the expansion of steam cavity and solidification will be finished only after the cavity expansion. The calculations by use of Eq. (55) are illustrated in Fig. 10.

Subsequent cooling of solid corium bubble will be accompanied by corresponding decrease in steam pressure inside the bubble. It is described by simple relation:

$$p_s(t) = p_0 \frac{T_{m0}}{T(t)} \tag{56}$$

where p_0 is the initial atmospheric pressure and T is the current temperature of the particle. When $T << T_{m0}$, the corium bubble will be compressed by external pressure and this effect can be considered by neglecting steam pressure inside the bubble. Assuming that the external pressure is equal to p_0, one can obtain the following estimate for hoop (circumferential) stress in the thin wall of the particle:

$$\sigma_\theta = \frac{p_0 r_e}{2\delta} \qquad \delta = r_e - r_{i,\max} \approx 3a^3 / r_e^2 \tag{57}$$

or

$$\sigma_\theta = \frac{p_0}{6}\left(\frac{r_e}{a}\right)^3 = \frac{\sqrt{3}}{2} p_0 \left(\frac{a}{\delta}\right)^{3/2} \tag{58}$$

In the case of thin-wall corium bubbles, this compressive hoop stress may be greater than the failure strength of the crust. It is especially dangerous in the case when the local external pressure during FCI's appears to be greater than the normal atmospheric pressure or there is an external shock of another nature. It may lead to the particle failure like that observed in laboratory experiments by Kudinov et al. [6].

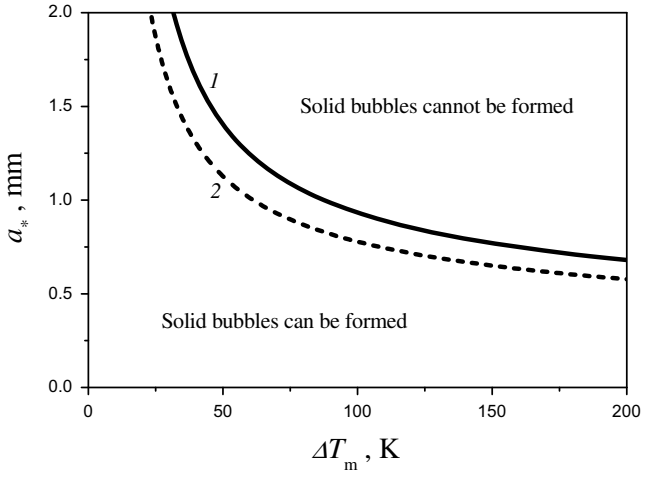

Fig. 9. The conditions of possible formation of hollow solid particles from corium (*1*) and low temperature melt (*2*). Calculations for water droplet of radius $r_{w0} = 50$ μm.

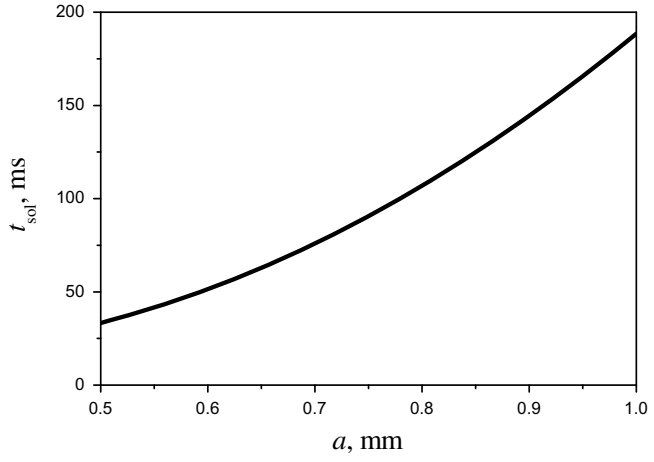

Fig. 10. Time of complete solidification of "corium bubble" as a function of initial radius of the melt droplet. Calculations for water droplet of radius $r_{w0} = 50$ μm.

6. Conclusions

A physical model of formation of thin-wall hollow solid particles in melt–coolant interaction is developed. The simplified mathematical formulation is based on quasi-steady isobaric approach for evaporation of small water droplet and expansion of steam cavity inside the original drop of the melt. The possibility of "solid bubble" formation depends on the correlation between the rates of steam cavity expansion and solidification of the expanding melt drop.

The computational analysis showed that large solid bubbles can be produced only at very small initial overheating of the melt. In the range of physical parameters corresponding to the interaction of the core melt with water pool, the calculations showed that only small corium droplets of diameter less than 1–2 mm can produce "solid bubbles". Numerical data for hypothetic low-temperature opaque melt indicated that formation of solid bubbles is weakly sensitive to the melting temperature and can be studied in experiments with simulant melts.

According to simple estimates, some of corium bubbles can be destroyed under the action of the external pressure after their cooling in ambient water. This result, as well as the predicted sizes of solid bubbles, is in qualitative agreement with recently reported laboratory observations.

Acknowledgements

This study was supported by the Royal Institute of Technology (KTH, Stockholm) and the Russian Foundation for Basic Research (Grant 07-08-00015). The author is also grateful to Professor A.P. Kryukov for useful discussions of the paper.

References

[1] M. Bürger, Particulate debris formation by breakup of melt jets, Nucl. Eng. Des. 236 (19–21) (2006) 1991–1997.
[2] D. Magallon, Characteristics of corium debris bed generated in large-scale fuel–coolant interaction experiments, Nucl. Eng. Des. 236 (19–21) (2006) 1998–2009.
[3] G. Pohlner, Z. Vujic, M. Bürger, G. Lohnert, Simulation of melt jet breakup and debris bed formation in water pools with IKEJET/IKEMIX, Nucl. Eng. Des. 236 (19–21) (2006) 2026–2048.
[4] M. Bürger, G. Berthoud, Basic laws and coolability of particulate debris: comments on the status and present contributions, Nucl. Eng. Des. 236 (19–21) (2006) 2049–2059.
[5] A. Karbojian, W. Ma, P. Kudinov, M. Davydov, N. Dinh, A scoping study of debris formation in DEFOR experimental facility, Proc. 15th Int. Conf. Nucl. Eng. (ICONE15), Nagoya, Japan, April 22–26, 2007, paper 10620.
[6] P. Kudinov, A. Karbojian, W. Ma, T.-N. Dinh, An experimental study on debris formation with corium simulant materials, Proc. Int. Cong. Adv. Nucl. Power Plants (ICAPP'08), Anaheim, CA, USA, June 8–12, 2008, paper 8390.
[7] L.A. Dombrovsky, Approximate model for break-up of solidifying melt particles due to thermal stresses in surface crust layer, Int. J. Heat Mass Transfer 52 (3–4) (2009) 582–587.
[8] M.K. Denham, A.P. Tyler, D.F. Fletcher, Experiments on the mixing of molten uranium dioxide with water and initial comparisons with CHYMES code calculations, Nucl. Eng. Des. 146 (1–3) (1994) 97–108.
[9] M.S. Plesset, R.B. Chapman, Collapse of an initially spherical vapor cavity in the neighbourhood of a solid boundary, J. Fluid Mech. 47 (2) (1971) 283–290.
[10] D.J. Buchanan, Model for fuel–coolant interactions, Phys. D: Appl. Phys. 7 (10) (1974) 1441–1458.
[11] B. Kim, M.L. Corradini, Modeling of small-scale single droplet fuel/coolant interactions, Nucl. Sci. Eng. 98 (1) (1988) 16–28.
[12] M.L. Corradini, B.J. Kim, M.D. Oh, Vapor explosion in light water reactors: a review of theory and modeling, Prog. Nucl. Energy 22 (1) (1988) 1–117.
[13] T.N. Dinh, A.T. Dinh, R.R. Nourgaliev, B.R. Sehgal, Investigation of film boiling thermal hydraulics under FCI conditions: results of analyses and numerical study, Nucl. Eng. Des. 189 (1–3) (1999) 251–272.
[14] A.P. Prishivalko, S.T. Leiko, Radiative heating and evaporation of droplets, J. Appl. Spectr. 33 (4) (1980) 1137–1143.
[15] A.P. Prishivalko, Heating and destruction of water drops on exposure to radiation with inhomogeneous internal heat evolution, Russ. Phys. J. 26 (2) (1983) 142–148.
[16] M.A. Sitarski, Thermal dynamics of a small vaporizing slurry droplet in a hot and radiant environment; feasibility of the secondary atomization, Combust. Sci. Tech. 71 (1–3) (1990) 53–75.
[17] P.L.C. Lage, C.M. Hackenberg, R.H. Rangel, Nonideal vaporization of dilating binary droplets with radiation absorption, Combust. Flame 101 (1) (1995) 36–44.
[18] L.G. Astafieva, A.P. Prishivalko, Heating of solid aerosol particles exposed to intense optical radiation, Int. J. Heat Mass Transfer 41 (2) (1998) 489–499.
[19] G. Miliauskas, Interaction of the transfer processes in semitransparent liquid droplets, Int. J. Heat Mass Transfer 46 (21) (2003) 41190–41380.
[20] C.C. Tseng, R. Viskanta, Heating/melting of a fused silica particle by convection and radiation, Int. J. Heat Mass Transfer 49 (17–18) (2006) 2995–3003.
[21] L.A. Dombrovsky, W. Lipiński, Transient temperature and thermal stress profiles in semi-transparent particles under high-flux irradiation, Int. J. Heat Mass Transfer 50 (11–12) (2007) 2117–2123.
[22] C.F. Bohren, D.R. Huffman, Absorption and Scattering of Light by Small Particles, Wiley, New York, 1983.
[23] L.A. Dombrovsky, Thermal radiation from nonisothermal spherical particles of a semitransparent material, Int. J. Heat Mass Transfer 43 (9) (2000) 1661–1672.
[24] L.A. Dombrovsky, A modified differential approximation for thermal radiation of semitransparent nonisothermal particles: Application to optical diagnostics of plasma spraying, J. Quant. Spectr. Radiat. Transfer 73 (2–5) (2002) 433–441.
[25] L.A. Dombrovsky, Absorption of thermal radiation in large semi-transparent particles at arbitrary illumination of the polydisperse system, Int. J. Heat Mass Transfer 47 (25) (2004) 5511–5522.
[26] G.M. Hale, M.P. Querry, Optical constants of water in the 200 nm to 200 μm wavelength region, Appl. Opt. 12 (3) (1973) 555–563.
[27] L.A. Dombrovsky, Radiation Heat Transfer in Disperse Systems, Begell House, New York, 1996.
[28] L.A. Dombrovsky, Radiative properties of particles and fibers, ThermalHUB publication. http://thermalhub.org/contributors/1050. 2008.
[29] L.A. Dombrovsky, S.S. Sazhin, A parabolic temperature profile model for heating of droplets, ASME J. Heat Transfer 125 (3) (2003) 535–537.
[30] L.A. Dombrovsky, S.S. Sazhin, A simplified nonisothermal model for droplet heating and evaporation, Int. Commun. Heat Mass Transfer 30 (6) (2003) 787–796.
[31] V.P. Skripov, Metastable Liquids, Wiley, New York, 1974.
[32] D.A. Labuntsov, A.P. Kryukov, Analysis of intensive evaporation and condensation, Int. J. Heat Mass Transfer 22 (7) (1979) 989–1002.
[33] T. Ytrehus, S. Østmo, Kinetic theory approach to interphase processes, Int. J. Multiphase Flow 22 (1) (1996) 133–155.
[34] J.W. Rose, Accurate approximate equations for intensive subsonic evaporation, Int. J. Heat Mass Transfer 43 (20) (2000) 3869–3875.
[35] L.A. Dombrovsky, L.I. Zaichik, The dynamics of vapor void under conditions of thermal interaction of a hot spherical particle with ambient water, High Temp. 38 (6) (2000) 938–947.
[36] L.A. Dombrovsky, An estimate of stability of large solidifying droplets in fuel–coolant interaction, Int. J. Heat Mass Transfer 50 (19–20) (2007) 3832–3836.
[37] L.A. Dombrovsky, T.N. Dinh, The effect of thermal radiation on the solidification dynamics of metal oxide melt droplets, Nucl. Eng. Des. 238 (6) (2008) 1421–1429.
[38] M.H. Yuan, Y.H. Yang, T.S. Li, Z.H. Hu, Numerical simulation of film boiling on a sphere with a volume of fluid interface tracking method, Int. J. Heat Mass Transfer 51 (7–8) (2008) 1646–1657.
[39] L.A. Dombrovsky, Large-cell model of radiation heat transfer in multiphase flows typical for fuel–coolant interaction, Int. J. Heat Mass Transfer 50 (17–18) (2007) 3401–3410.
[40] L.A. Dombrovsky, M.V. Davydov, P. Kudinov, Thermal radiation modeling in numerical simulation of melt–coolant interaction, Proc. Int. Symp. Adv. Comput. Heat Transfer (CHT-08), Marrakech, Morocco, May 11–16, 2008, paper 155.
[41] L.A. Dombrovsky, M.V. Davydov, P. Kudinov, Thermal radiation modeling in numerical simulation of melt–coolant interaction, Comp. Therm. Sci. 1 (1) (2009), in press.